# Highly Selective Detection of Trinitrophenol by Luminescent Functionalized Reduced Graphene Oxide through FRET Mechanism

Diptiman Dinda, Abhisek Gupta, Bikash Kumar Shaw, Suparna Sadhu, and Shyamal Kumar Saha*

Department of Materials Science, Indian Association for the Cultivation of Science, Jadavpur, Kolkata 700032, India

Ⓢ Supporting Information

**ABSTRACT:** Among different nitro compounds, trinitrophenol (TNP) is the most common constituent to prepare powerful explosives all over the world. A few works on the detection of nitro explosives have already been reported in the past few years; however, selectivity is still in its infant stage. As all the nitroexplosives are highly electron deficient in nature, it is very difficult to separate one from a mixture of different nitro compounds by the usual photoinduced electron transfer (PET) mechanism. In the present work, we have used a bright luminescent, 2,6-diamino pyridine functionalized graphene oxide (DAP-RGO) for selective detection of TNP in the presence of other nitro compounds. The major advantage of using this material over other reported materials is not only to achieve very high fluorescence quenching of ~96% but also superior selectivity >80% in the detection of TNP in aqueous medium via both fluorescence resonance energy transfer and PET mechanisms. Density functional theory calculations also suggest the occurrence of an effective proton transfer mechanism from TNP to DAP-RGO, resulting in this tremendous fluorescence quenching compared to other nitro compounds. We believe this graphene based composite will emerge a new class of materials that could be potentially useful for selective detection, even for trace amounts of nitro explosives in water.

**KEYWORDS:** selective detection, nitro explosives, luminescent, graphene oxide, FRET
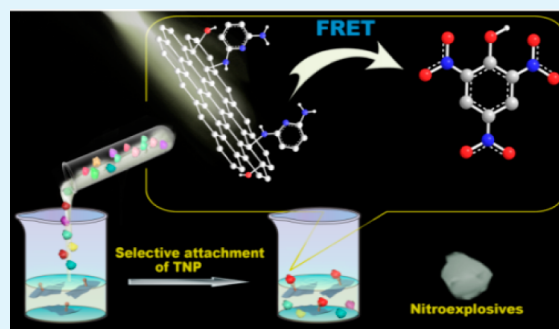
## INTRODUCTION

Now-a-days, instant and selective detection of trace amounts of explosives has become a burning issue due to increasing demand for homeland security at different places like airports, mail storing centers, transit centers for civilians, military applications and also for forensic investigations.[1,2] Several methods are used to detect those explosives like surface plasma resonance, field effect transition, portable mass spectrometry, ion mobility spectrometry, X-ray systems, electrochemical methods, microcantilever and optical based sensing.[3−7] Among them, fluorescence based optical sensing is one of the finest techniques to detect those nitro explosives and has become very popular because of its simple instrumentation, cost-efficiency, fast and high sensitivity.[8,9]

Generally, nitro aromatic derivatives are being used worldwide to prepare different explosives.[10] Among them, the detection of 2,4,6-trinitrophenol (TNP) has become very popular as it is much more explosive than others. Due to its higher water solubility, it contaminates groundwater and soil and causes irritants in the skin, eyes and respiratory system.[11] As all the nitro explosives show strong electron affinity, it is very difficult to separate TNP from a mixture of other nitro compounds. Hence, development of an efficient selective sensor for the detection of TNP is highly desirable. Although, some reported materials like metal−organic frameworks and π-conjugated polymers show good sensitivity toward nitro-explosives but selectivity in aqueous medium is still unex-

plored.[12−14] Therefore, high selectivity as well as excellent fluorescence quenching toward sensing of superior explosive TNP in water medium is an emerging field.

Graphene, a two-dimensional honeycomb-like carbon lattice, has become very popular due to its unique properties. From an electronic and structural point of view, it is believed that functionalized graphene oxide (GO) has also a very good sensing ability toward nitroexplosives. Very few works on graphene based composites have been reported to detect nitro explosives but they do not possess good selectivity.[15−18] Exploiting the large surface area of graphene, we have synthesized 2,6-diamino pyridine functionalized graphene oxide (DAP-RGO) using simple $S_N2$ reaction at basal epoxy sites of GO as reported in our previous work.[19] Our prepared material gives a bright photoluminescence (PL) spectrum that we have used in the present work to detect superior explosive TNP selectively in aqueous medium.

We have achieved a remarkably high (96%) fluorescence quenching efficiency with very good selectivity (>80%) toward the detection of TNP in water medium. The advantage of using this material is to distinguish TNP in the presence of other nitro explosives by the fluorescence resonance energy transfer (FRET) mechanism in addition to photoinduced electron

transfer (PET), which alone cannot give such a remarkable selectivity. Furthermore, we can easily detect very trace amounts of TNP (125 ppb) in aqueous medium using our material as a sensor. Here, graphene oxide helps to attach a large number of DAP moieties on its high surface area, which facilitates very strong electrostatic interaction between host and guest by proton transfer from acidic TNP to the basic sites of DAP-RGO moiety, resulting in very pronounced and selective fluorescence quenching compared to other nitro explosives. The density functional theory (DFT) calculations also help us to understand the nature of the interactions between fluorophore DAP-RGO and TNP for its superior selectivity. Thus, predominant FRET and efficient electrostatic interaction facilitates this remarkably high selectivity of DAP-RGO toward detection of TNP over other nitro explosives in a mixture.

## ■ RESULTS AND DISCUSSION

**Photoluminescence Study.** The as-synthesized GO shows very weak emission bands at ~438 and 500 nm using the excitation wavelength at 360 nm as shown in Figure 1. Due to
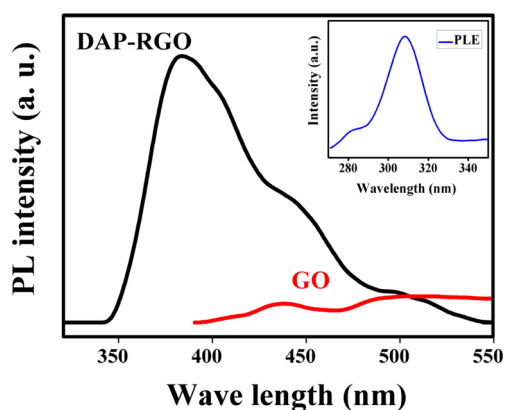


**Figure 1.** Comparison of PL between DAP-RGO composite and GO and inset shows the PLE spectra of DAP-RGO.

the presence of large numbers of oxygen containing functional groups, each graphene oxide sheet is considered as the combination of sp$^2$ carbon nanoclusters embedded in sp$^3$ matrix. So, structurally disorder induced localized states appear within the π−π* gap, resulting in a broad emission peak in the range of 500−800 nm as a result of optical transitions among those localized states.[20,21] Besides this, a comparatively sharper peak is observed at ~438 nm due to a π-conjugated island of the sp$^2$ hybridized carbon network in the GO.

But, our prepared material (DAP-RGO) shows an intense blue-shifted PL spectrum at ~384 nm when excited at 309 nm wavelength. The intensity of this PL spectrum is very large (900%) w.r.to the PL of graphene oxide. The corresponding PLE spectrum of this material also shows a strong peak at 308 nm (inset of Figure 1). This bright PL spectra is attributed to the surface passivation of GO during functionalization with aromatic amine. The epoxy groups usually incorporate localized nonradiative electron−hole (e−h) pairs in GO leading to very weak emission spectra. With the treatment of alkyl or aromatc amines, these nonradiative sites are removed through nucleophilic reactions. Then nonemissive GO sheets are transformed into a highly efficient emitter.[22,23] Photolumines-cent quantum yields for GO and DAP-RGO are also calculated using a standard dye (quinine sulfate in 0.1 M H$_2$SO$_4$) to

compare this kind of large increments in PL intensity (given in the Supporting Information). It shows 18.67% QY where GO gives only 0.03%, which fully supports our results. DAP-RGO also shows an excitation dependent PL property, which arises due to the surface passivation during functionalization (Figure S6, Supporting Information).

**Nitroexplosive Sensing in Aqueous Medium.** To explore this superior photoluminescence property toward the selective detection of nitro aromatic explosives, we have examined the fluorescence quenching titrations by adding the aqueous solution of nitro explosives gradually to the aqueous solution of DAP-RGO composite. Quite large fluorescence quenching is observed after immediate addition of 25 μL 1 mM TNP solution and it reaches to 96% upon addition of 200 μL 1 mM TNP solution (Figure 2).
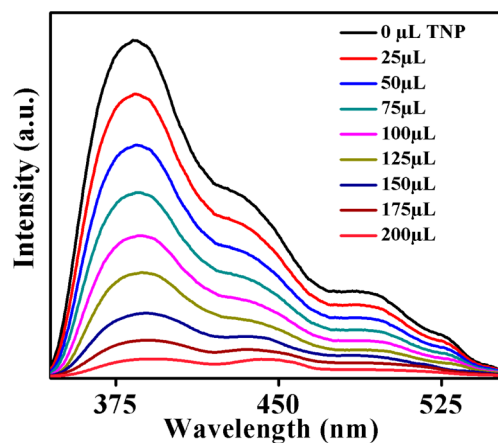


**Figure 2.** Fluorescence quenching of DAP-RGO after gradual addition of different amounts of 1 mm TNP solution at buffer 7.

To check the selectivity of DAP-RGO toward TNP, we have also performed this fluorescence quenching titration experiment with other nitro compounds such as 2,6-DNT, 2,4-DNT, 1,4-DNB, 1,3-DNB, 1,2-DNB; 4-NT, 2-NT and NB. All these compounds show very weak quenching efficiency compared to that of TNP as shown in Figures 3a and S7−14 (Supporting Information). These results indicate the selectivity of DAP-RGO toward TNP.

Furthermore, the fluorescence quenching efficiency is analyzed by Stern−Volmer eq 1

$$I_0/I = K_{S-V}[Q] + 1 \tag{1}$$

where $I_0$ and $I$ are fluorescence intensities before and after addition of nitro explosive, $[Q]$ is the molar concentration of analytes added and $K_{S-V}$ is the quenching constant (M$^{-1}$). From Figure 3b, it is seen that TNP shows an exponential S−V curve whereas others show a linear curve. At lower concentrations, the Stern−Volmer plot of TNP is close to linear but, for higher concentration, it deviates from linearity and increases almost exponentially. For other nitro compounds, the plots also remain linear at higher concentrations.

This kind of nonlinear plot for TNP suggests an effective energy transfer mechanism (FRET) operated in its quenching process with respect to others.[24,25] The quenching constant value for TNP is 1.305 × 10$^5$ M$^{-1}$, calculated using an exponential quenching eq 2[26]

$$I_0/I = Ae^{K[Q]} + B \tag{2}$$
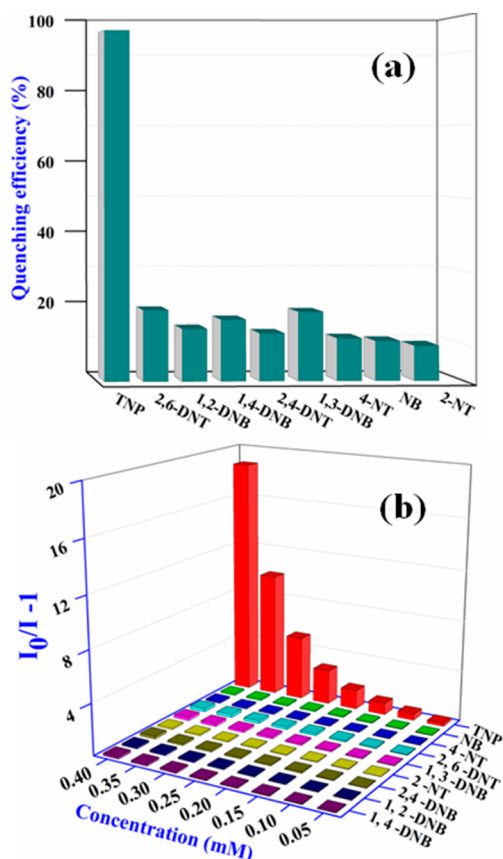
**Figure 3.** (a) Quenching efficiency of DAP-RGO toward different nitro aromatic compounds after addition of 200 μL of 1 mM TNP solution at buffer 7 and (b) Stern−Volmer plot for all nitro compounds.

which is quite larger than the previous reported results (Table S1, Supporting Information). The quenching constant values for all the nitroexplosives are given in Table 1. From Table 1, it is observed that $K_{SV}$ values for TNP are quite larger than those for other nitro explosives, suggesting very predominant selectivity of TNP from others.

**Table 1. Fluorescence Quenching Constant ($K_{S-V}$) Values for Different Nitro Explosives**

| analytes | $K_{S-V}$ values | correlation coefficient ($R^2$) |
|---|---|---|
| TNP | $1.322 \times 10^5$ | >.999 |
| 2,4-DNT | $3.539 \times 10^3$ | >.997 |
| 2,6-DNT | $6.199 \times 10^3$ | >.988 |
| 1,2-DNB | $4.021 \times 10^3$ | >.99 |
| 1,3-DNB | $5.662 \times 10^3$ | >.999 |
| 1,4-DNB | $4.526 \times 10^3$ | >.99 |
| 4-NT | $3.167 \times 10^3$ | 0.996 |
| 2-NT | $2.315 \times 10^3$ | 0.993 |
| NB | $2.843 \times 10^3$ | 0.987 |

**Selectivity Titration.** To confirm the selectivity of DAP-RGO toward TNP, we have also studied the quenching titration experiment in the presence of other nitro compounds. The aqueous solution of 2,6-DNT is added initially to the aqueous solution of DAP-RGO to access most of the binding sites of the composite followed by TNP and the same process is carried-out for other nitro aromatics. The experimental results

show that 2,6-DNT initially gives very weak quenching of PL whereas it increases drastically upon addition of TNP and remains almost unaltered after further addition of 2,6-DNT. Similar kinds of results are also noticed for the other nitro aromatics. We have plotted the stepwise increase of quenching efficiency against the gradual addition of nitro aromatic analytes in the presence of TNP (Figure 4). This experiment confirms very high selectivity of DAP-RGO toward TNP.
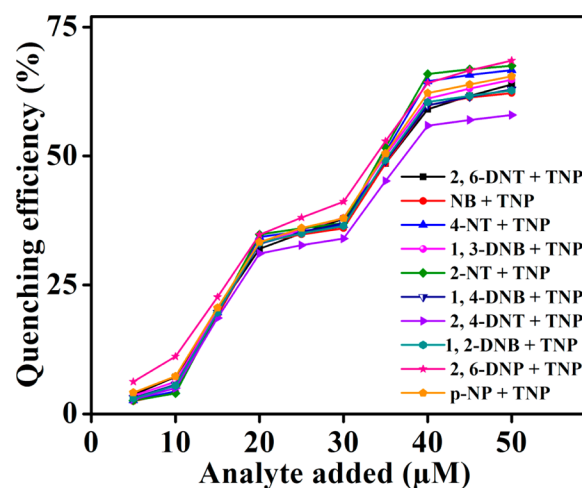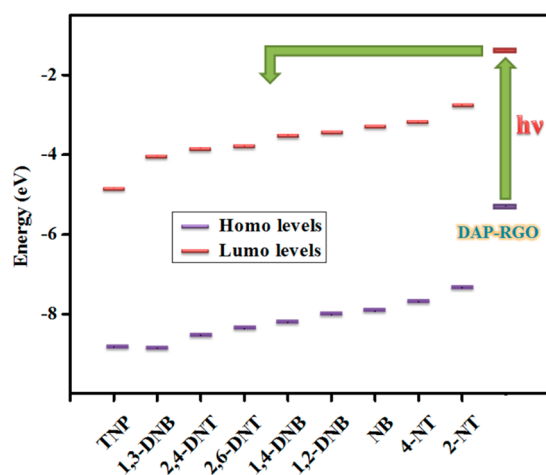


**Figure 4.** Increase in the fluorescence quenching efficiency upon addition of different nitro compounds followed by TNP at buffer 7.

It is seen that our material is highly sensitive toward TNP and can detect very low concentration of TNP. Calculated detection limit of TNP is ∼125 ppb for our material. All the calculations and graph (Figure S15) are given in Supporting Information.

**Mechanism for Selective Detection.** To investigate the origin of high selectivity of DAP-RGO toward TNP compared to other nitro aromatics, we have studied the quenching mechanism process. The fluorescence quenching process mainly occurs in two ways (i) PET and (ii) FRET mechanisms. During the PET mechanism, electrons are first excited from the electron rich HOMO of the DAP-RGO composite to its LUMO and then transferred to the LUMO of electron deficient nitro compounds causing fluorescence quenching. The energy gap between the LUMOs of donor fluorophore (DAP-RGO) and acceptor nitro compounds is the main driving force for this transition.[27,9] We have investigated the corresponding HOMO−LUMO energy levels for all the nitro aromatics as well as DAP-RGO (Table S2, Supporting Information) by DFT technique using the B3LYP/6-31G* method in the GAUS-SIAN 03 software package to check this effect. The decreasing LUMO energy levels of nitro aromatics as shown in Figure 5 represent how easily excited electrons are transferred from the higher energy LUMO of the DAP-RGO composite to the lower energy LUMO of electron-deficient nitro aromatics. Although TNP has the lowest LUMO energy level, the quenching efficiency of all nitro aromatics is not well in agreement with this band energy difference. This clarifies that the PET process is not the only factor showing such highly selective fluorescence quenching toward TNP.

The nonlinear S−V plot of TNP shown in Figure 3b suggests the FRET process occurs between them. If the emission band of the fluorophore overlaps effectively with the absorption band of the nitro aromatics, then the FRET mechanism is operated

10724

dx.doi.org/10.1021/am5025676 | ACS Appl. Mater. Interfaces 2014, 6, 10722−10728

**Figure 5.** Energy profile diagram for different nitro explosives with increasing LUMO energy levels during the PET mechanism.

from fluorophore to nitro aromatics, resulting in a large fluorescence quenching compared to PET, as the efficiency of FRET is quite higher than that of PET based fluorescence quenching.[28,29] From Figure 6, it is clear that the absorption
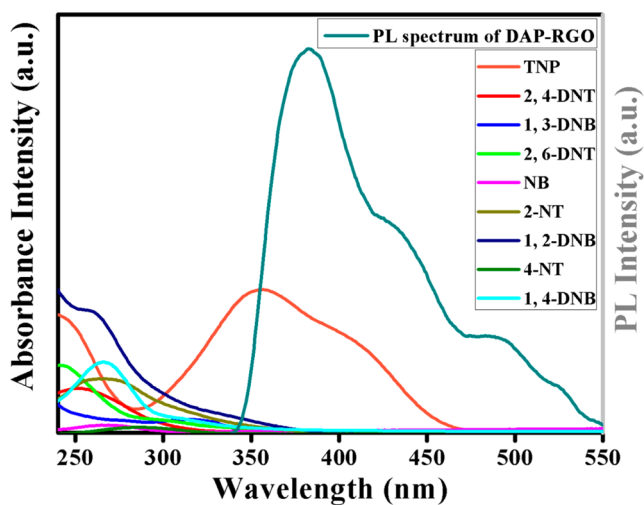


**Figure 6.** Spectral overlap between emission spectrum of DAP-RGO and absorption spectra of different nitroexplosive compounds.

band of TNP quite effectively overlaps with the emission band of DAP-RGO, resulting in this kind of dramatic fluorescence quenching compared to other nitro aromatic explosives that have poor overlaps. Overlap integral values for all the nitro compounds are also calculated using eq 3[30]

$$J(\lambda) = \int_0^\infty F_D(\lambda)\varepsilon_A(\lambda)\lambda^4 d\lambda \qquad (3)$$

where $F_D(\lambda)$ is the corrected fluorescence intensity of donor in the range of $\lambda$ to $\lambda + \Delta\lambda$ with the total intensity normalized to unity, and $\varepsilon_A$ is extinction coefficient of the acceptor at $\lambda$ in $M^{-1}$ $cm^{-1}$. Maximum overlap is observed for TNP with overlap integral $2.526\,425 \times 10^{14}$, which is 18 times larger than that for 2,6-DNT and 147 times greater than that for 1,3-DNB. All the overlap integral values for different nitro compounds are given in Table 2. These statistics confirms the selectivity of DAP-RGO toward TNP.

**Table 2. Overlap Integral $J(\lambda)$ Values for Different Explosives**

| different nitro compounds | $J(\lambda)$ values ($M^{-1}$ $cm^{-1}$ $nm^4$) |
|---|---|
| TNP | $2.5264 \times 10^{14}$ |
| 2,4-DNT | $7.0829 \times 10^{12}$ |
| 2,6-DNT | $1.3926 \times 10^{13}$ |
| 1,2-DNB | $2.4945 \times 10^{13}$ |
| 1,3-DNB | $1.7108 \times 10^{12}$ |
| 1,4-DNB | $1.34216 \times 10^{13}$ |
| 4-NT | $1.01674 \times 10^{12}$ |
| 2-NT | $5.1267 \times 10^{11}$ |
| NB | $6.2894 \times 10^{11}$ |

**Time Resolved Fluorescence Study.** To confirm the occurrence of energy transfer from DAP-RGO to TNP molecules, a time-correlated single-photon counting (TCSPC) study is performed because of the fact that decay time measurements are more sensitive than fluorescence quenching efficiencies. We use a pulsed excitation of 340 nm to measure the decay times of our DAP-RGO material before and after addition of TNP. From Figure S16 (Supporting Information), we can see that a sharp decrease in decay time is observed for DAP-RGO after the addition of TNP. This decrease in average lifetime confirms the energy transfer (FRET) from DAP-RGO to TNP. The energy transfer efficiency is also calculated using eq 4[30]

$$\phi_{ET} = 1 - \tau_{D-A}/\tau_D \qquad (4)$$

where $\phi_{ET}$ is the calculated FRET efficiency, $\tau_{D-A}$ is the decay time for DAP-RGO in the presence of TNP and $\tau_D$ corresponds to the decay time for pure DAP-RGO. The calculated energy transfer efficiency achieved is ~48% for TNP. We have also calculated the donor−acceptor and Förster distances ($r$, $R_0$ respectively) using eqs 5 and 6 given below.[30]

$$R_0 = 0.211[k^2 n^{-4}\Phi_D J(\lambda)] \text{ in Å units} \qquad (5)$$

$$\phi_{ET} = 1/1 + (r/R_0)^6 \qquad (6)$$

where $k^2$ is the orientation factor of two interacting dipoles and is usually assumed to be 2/3, $\Phi_D$ is the quantum efficiency of the donor, $J(\lambda)$ is the overlap integral between the absorption peak of the acceptor and emission peak of the donor and $n$ is the refractive index of the medium. From Table 3, it is seen that the donor−acceptor distance for our system is 31.4 Å, which is well inside the range of 10 to 100 Å for FRET.

**Table 3. Energy Transfer Parameters for DAP-RGO/TNP System Using FRET Method**

| system | $\tau_{avg}$ (ns) | $\phi_{ET}$ (%) | $r$ (Å) | $R_0$ (Å) |
|---|---|---|---|---|
| DAP-RGO | 3.724 | | | |
| DAP-RGO + TNP | 1.935 | 48 | 31.02 | 31.44 |

**Features of Association Complex Formation.** Selectivity of TNP sensing can also be explained from the electrostatic interaction between a fluorophore (DAP-RGO) and TNP compared to other nitro aromatics. As TNP is acidic in nature, it can easily exchange a proton to the highly basic pyridine nitrogen of the fluorophore and forms an electrostatic association complex with TNP as shown in Scheme1. This kind of interaction further promotes electron transfer from electron rich DAP-RGO to the highly electrodeficient TNP,

**Scheme 1. Schematic Picture of Proton Transfer from TNP to Pyridinic Nitrogen of DAP-RGO**
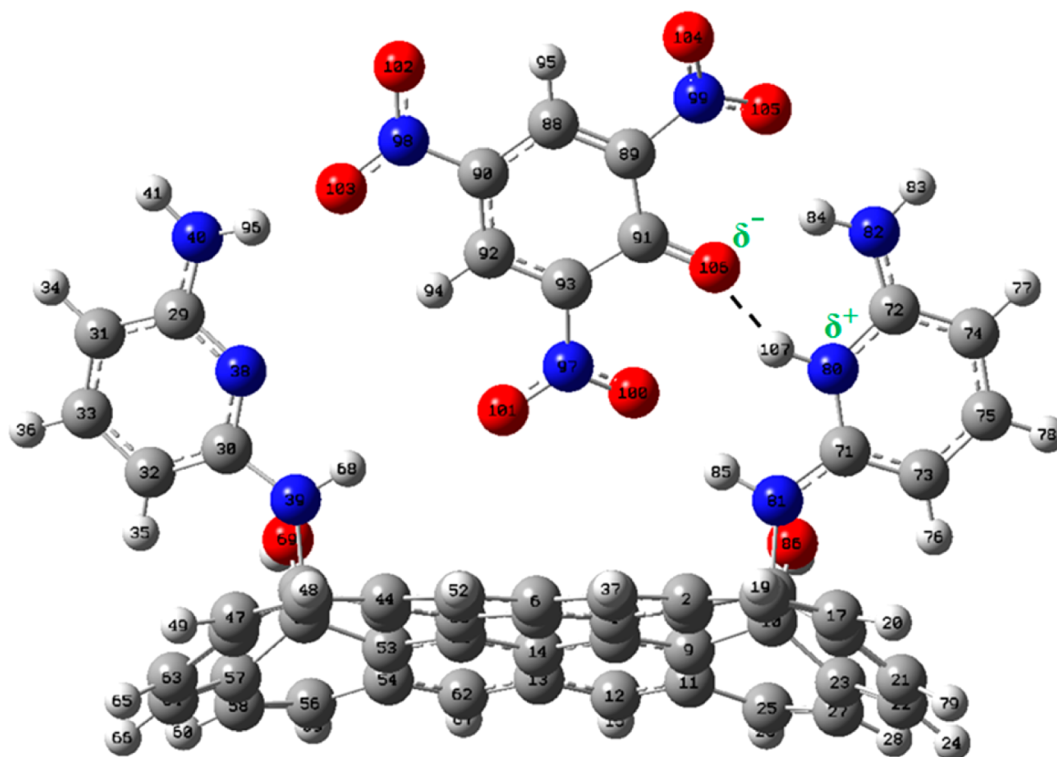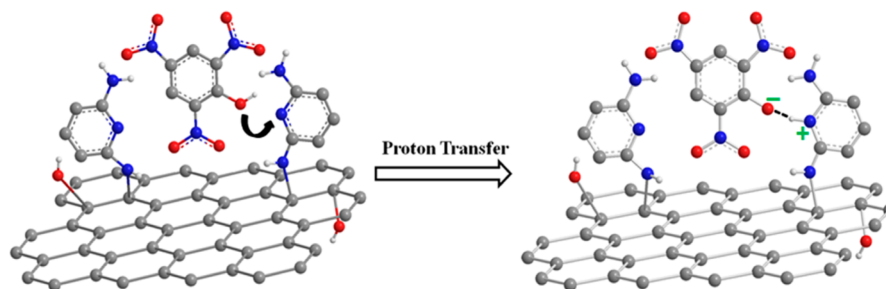




Figure 7. DFT optimized complex between TNP and DAP-RGO.

causing large fluorescence quenching.[31,32] The appearance of a new absorption band at 410 nm in the UV−vis spectrum (Figure S17, Supporting Information) of DAP-RGO after addition of TNP also confirms this effect.[33] We have also checked theoretically whether this kind of proton transfer occurs from different nitro aromatics to DAP-RGO using DFT calculation. The optimized structure in Figure 7 and calculated interactive distances in Table S3 (Supporting Information) confirm that this kind of proton transfer only occurs from TNP to DAP-RGO, leading to the formation of an association complex. However, no such proton transfer is observed in the case of 2,6-DNT, as shown in Figure S18 and Table S4 (Supporting Information).

To confirm whether this kind of acid−base interaction happened in the case of TNP, we have also carried out fluorescence quenching experiments with some other nitro compounds like 2,6-dinitro phenol, 2,4-dinitro phenol and 4-nitrophenol, which contain one hydroxyl group. The quenching efficiency is in descending order like TNP≫ 2,4-DNP> 2,6-DNP> p-NP, which is in accordance with their acidic nature. The quenching efficiency of 2,4-DNP; 2,6-DNP and p-NP are also quite higher (Figures S19−21, Supporting Information)

than their isomeric nitro compounds. As isomeric nitro compounds do not contain any hydroxyl group, they cannot interact strongly with the basic sites of fluorophore, giving some weak quenching response. TNP, being highly acidic in nature, can strongly interact with the basic sites of DAP-RGO and shows such amplified quenching response.[25]

Thus, predominantly FRET, efficient electrotransfer and suitable electrostatic interaction guide this unprecedented selectivity of TNP in spite of other nitro aromatic compounds.

## ■ CONCLUSION

In summary, we have synthesized 2,6-diamino pyridine functionalized GO (DAP-RGO) through a simple reaction route and enhanced the weak PL intensity of GO dramatically by ~900%. Using this material as a fluorophore, we successfully demonstrate the selective detection of the superior nitro explosive TNP in aqueous medium in the presence of other nitro explosives. We also theoretically prove the selective attachment of TNP with basic sites of the fluorophore, which results in such anomalous selectivity of DAP-RGO toward TNP sensing. We believe that this study will emerge an effective way

for selective detection of modern nitro explosives under very realistic conditions in the near-future.

# EXPERIMENTAL SECTION

**Materials.** All the nitro aromatics (structures given in Scheme S1, Supporting Information) are obtained from Sigma-Aldrich and they are used very carefully for the experiments. 2,6-Diamino pyridine (DAP) is also obtained from Sigma. All other reagents like graphite powder, sodium hydroxide, hydrogen peroxide (30%), methanol (99%), sulfuric acid (98 wt %), ammonia solution (25%), potassium permanganate, sodium chloride, sodium nitrite, etc. are purchased from Merck Chemicals.

**Chemical Synthesis.** Graphene oxide (GO) is prepared from graphite powder by modified Hummers method. Then 20 mL of GO is sonicated with 100 mL of distilled water for homogeneous dispersion. After that, 500 mg of DAP is added to this solution followed by ammonia and stirred for 4 h under heating conditions to obtain DAP-RGO composite shown in Scheme S2 (Supporting Information) according to our previous report.

**Characterizations.** Fourier transform infrared spectroscopy (FTIR) and X-ray photoelectron spectroscopy (XPS) measurements of the DAP-RGO composites are carried out using a NICOLET MAGNA IR 750 system and OMICRON-0571 system, respectively. A thermogravimetric analysis (TGA) experiment is also conducted with a SDT Q600 V20.5 Build 15 at a heating rate of 10 °C/min from 25−800 °C in $N_2$ atmosphere. UV−vis and all the fluorescence experiments are carried out with a SHIMADZU-1601 UV−vis and Horiba Jobin Yvon Fluoromax-4 spectrofluorometer.

Powder X-ray diffraction (XRD) measurements are carried out using powdered samples with an X-ray diffractometer (RICH SEIFERT-XRD 3000P with X-ray Generator-Cu, 10 kV, 10 mA, wavelength 1.5418 Å). All the Microstructural analysis of this material are given in the Supporting Information, Figures S1−5.

**Fluorescence Quenching Experiments.** Fluorescence quenching experiments are carried out dispersing 1 mg of DAP-RGO composite in 2.5 mL of solution in a quartz tube upon excitation at 309 nm wavelength using buffer 7. All the titration experiments are done adding 1 mM of different nitro explosive analytes solutions dropwise in an increasing order gradually to this solution of buffer 7. All the measurements are carried out in triplicate form and all the results are in good agreements.

# ASSOCIATED CONTENT

## Ⓢ Supporting Information

Structures of nitrocompounds, synthesis and characterizations of the material, quantum yield calculations, photoluminescence study and PL quenching titration experiments, detection limit calculations, lifetime decays and PL quenching for different nitro phenols. This material is available free of charge via the Internet at http://pubs.acs.org.

# AUTHOR INFORMATION

## Corresponding Author

*S. K. Saha. Email: cnssks@iacs.res.in.

## Notes

The authors declare no competing financial interest.

# ACKNOWLEDGMENTS

# REFERENCES

(1) McQuade, D. T.; Pullen, A. E.; Swager, T. M. Conjugated Polymer-Based Chemical Sensors. *Chem. Rev.* **2000**, *100*, 2537.

(2) Toal, S. J.; Trogler, W. C. Polymer Sensors for Nitroaromatic Explosives Detection. *J. Mater. Chem.* **2006**, *16*, 2871.

(3) Aguilar, A. D.; Forzani, E. S.; Leright, M.; Tsow, F.; Cagan, A.; AIglesias, R.; Nagahara, L. A.; Amlani, I.; Tsui, R.; Tao, N. J. A Hybrid Nanosensor for TNT Vapor Detection. *Nano Lett.* **2010**, *10*, 380−384.

(4) McNeil, S. K.; Kelley, S. P.; Beg, C.; Cook, H.; Rogers, R. D.; Nikles, D. E. Cocrystals of 10-Methylphenthiazine and 1,3-Dinitrobenzene: Implications for the Optical Sensing of TNT-Based Explosives. *ACS Appl. Mater. Interfaces* **2013**, *5*, 7647−7653.

(5) Zu, B.; Guo, Y.; Dou, X. Nanostructure-Based Optoelectronic Sensing of Vapor Phase Explosives − a Promising but Challenging Method. *Nanoscale* **2013**, *5*, 10693−10701.

(6) Forzani, E. S.; Lu, D.; Leright, M. J.; Aguilar, A. D.; Tsow, F.; Iglesias, R. A.; Zhang, Q.; Lu, J.; Li, J. H.; Tao, N. J. A hybrid Electrochemical-Colorimetric Sensing Platform for Detection of Explosives. *J. Am. Chem. Soc.* **2009**, *131*, 1390.

(7) Kandpal, M.; Bandela, A. K.; Hinge, V. K.; Rao, V. R.; Rao, C. P. Fluorescence and Piezoresistive Cantilever Sensing of Trinitrotoluene by an Upper-Rim Tetrabenzimidazole Conjugate of Calix[4]arene and Delineation of the Features of the Complex by Molecular Dynamics. *ACS Appl. Mater. Interfaces* **2013**, *5*, 13448−13456.

(8) Andrew, T. L.; Swager, T. M. A Fluorescence Turn-On Mechanism to Detect High Explosives RDX and PETN. *J. Am. Chem. Soc.* **2007**, *129*, 7254.

(9) Xu, H.; Liu, F.; Cui, Y.; Chen, B.; Qian, G. A. Luminescent Nanoscale Metal−Organic Framework for Sensing of Nitroaromatic Explosives. *Chem. Commun.* **2011**, *47*, 3153−3155.

(10) Germain, M. E.; Knapp, M. Optical Explosives Detection: from Color Changes to Fluorescence Turn-On. *J. Chem. Soc. Rev.* **2009**, *38*, 2543−2555.

(11) U.S. Environmental Protection Agency. *Innovative Treatment Technologies: Annual Status Report*, 8th ed.; U.S. Environmental Protection Agency: Washington, D.C., 1996.

(12) Gao, D. M.; Wang, Z. Y.; Liu, B. H.; Ni, L.; Wu, M. H.; Zhang, Z. P. Resonance Energy Transfer-Amplifying Fluorescence Quenching at the Surface of Silica Nanoparticles toward Ultrasensitive Detection of TNT. *Anal. Chem.* **2008**, *80*, 8545.

(13) Yildirim, A.; Acar, H.; Erkal, T. S.; Bayindir, M.; Guler, M. O. Template-Directed Synthesis of Silica Nanotubes for Explosive Detection. *ACS Appl. Mater. Interfaces* **2011**, *3*, 4159−4164.

(14) Zhang, C.; Che, Y.; Zhang, Z.; Yang, X.; Zang, L. Fluorescent Nanoscale Zinc(II)-Carboxylate Coordination Polymers for Explosive Sensing. *Chem. Commun.* **2011**, *47*, 2336−2338.

(15) Guo, L.; Zu, B.; Yang, Z.; Caoa, H.; Zheng, X.; Dou, X. APTS and RGO Co-Functionalized Pyrenated Fluorescent Nanonets for Representative Vapor Phase Nitroaromatic Explosive Detection. *Nanoscale* **2014**, *6*, 1467−1473.

(16) Guo, C. X.; Lei, Y.; Li, C. M. Porphyrin Functionalized Graphene for Sensitive Electrochemical Detection of Ultratrace Explosives. *Electroanalysis* **2011**, *23*, 885−893.

(17) Lu, X.; Qi, H.; Zhang, X.; Xue, Z.; Jin, J.; Zhou, X.; Liu, X. Highly Dispersive Ag Nanoparticles on Functionalized Graphene for an Excellent Electrochemical Sensor of Nitroaromatic Compounds. *Chem. Commun.* **2011**, *47*, 12494.

(18) Zhou, X.; Yuan, C.; Qin, D.; Xue, Z.; Wang, Y.; Du, J.; Ma, L.; Ma, L.; Lu, X. Pd Nanoparticles on Functionalized Graphene for Excellent Detection of Nitro aromatic Compounds. *Electrochim. Acta* **2014**, *119*, 243−250.

(19) Dinda, D.; Gupta, A.; Saha, S. K. Removal of Toxic Cr(VI) by UV-Active Functionalized Graphene Oxide for Water Purification. *J. Mater. Chem. A* **2013**, *1*, 11221−11228.

(20) Luo, Z. T.; Vora, P. M.; Mele, E. J.; Johnson, A. T. C.; Kikkawa, J. M. Photoluminescence and Band Gap Modulation in Graphene Oxide. *Appl. Phys. Lett.* **2009**, *94*, 111909.

(21) Sun, X. M.; Liu, Z.; Welsher, K.; Robinson, J. T.; Goodwin, A.; Zaric, S.; Dai, H. J. Nano-Graphene Oxide for Cellular Imaging and Drug Delivery. *Nano Res.* **2008**, *1*, 203−212.

10727

dx.doi.org/10.1021/am5025676 | *ACS Appl. Mater. Interfaces* 2014, 6, 10722−10728

(22) Eda, G.; Lin, Y.; Mattevi, C.; Yamaguchi, H.; Chen, H.; Chen, I.; Chen, C.; Chhowalla, M. Blue Photoluminescence from Chemically Derived Graphene Oxide. *Adv. Mater.* **2010**, *22*, 505−509.

(23) Mei, Q.; Zhang, K.; Guan, G.; Liu, B.; Wang, S.; Zhang, Z. Highly Efficient Photoluminescent Graphene Oxide with Tunable Surface Properties. *Chem. Commun.* **2010**, *46*, 7319−7321.

(24) Salinas, Y.; Martinez-Manez, R.; Marcos, M. D.; Sancenon, F.; Castero, A. M.; Parra, M.; Gil, S. Optical Chemosensors and Reagents to Detect Explosives. *Chem. Soc. Rev.* **2012**, *41*, 1261−1296.

(25) Nagarkar, S. S.; Joarder, B.; Chaudhari, A. K.; Mukherjee, S.; Ghosh, S. K. Highly Selective Detection of Nitro Explosives by a Luminescent Metal−Organic Framework. *Angew. Chem., Int. Ed.* **2013**, *52*, 2881−2885.

(26) Feng, H.-T.; Zheng, Y.-S. Highly Sensitive and Selective Detection of Nitrophenolic Explosives by Using Nanospheres of a Tetraphenylethylene Macrocycle Displaying Aggregation-Induced Emission. *Chem.—Eur. J.* **2014**, *20*, 195−201.

(27) Sanchez, J. C.; Pasquale, A. G. D.; Rheingold, A. L.; Trogler, W. C. Synthesis, Luminescence Properties, and Explosives Sensing with 1,1-Tetraphenylsilole- and 1,1-Silafluorene-Vinylene Polymers. *Chem. Mater.* **2007**, *19*, 6459−6470.

(28) Tu, R.; Liu, B.; Wang, Z.; Gao, D.; Wang, F.; Fang, Q.; Zhang, Z. Amine-Capped ZnS−Mn$^{2+}$ Nanocrystals for Fluorescence Detection of Trace TNT Explosive. *Anal. Chem.* **2008**, *80*, 3458−3465.

(29) Wang, Y.; La, A.; Brückner, C.; Lei, Y. FRET- and PET-Based Sensing in a Single Material: Expanding the Dynamic Range of an Ultra-Sensitive Nitroaromatic Explosives Assay. *Chem. Commun.* **2012**, *48*, 9903−9905.

(30) Lakowicz, J. R. *Principles of Florescence spectroscopy*, 3rd ed; Springer: Singapore, 2010; pp 443−472.

(31) Bhalla, V.; Gupta, A.; Kumar, M.; Rao, D. S. S.; Prasad, S. K. Self-Assembled Pentacenequinone Derivative for Trace Detection of Picric Acid. *ACS Appl. Mater. Interfaces* **2013**, *5*, 672−679.

(32) Dey, N.; Samanta, S. K.; Bhattacharya, S. Selective and Efficient Detection of Nitro-Aromatic Explosives in Multiple Media Including Water, Micelles, Organogel, and Solid Support. *ACS Appl. Mater. Interfaces* **2013**, *5*, 8394−8400.

(33) Bhalla, V.; Kaur, S.; Vij, V.; Kumar, M. Mercury-Modulated Supramolecular Assembly of a Hexaphenylbenzene Derivative for Selective Detection of Picric Acid. *Inorg. Chem.* **2013**, *52*, 4860−4865.